

This work was written as part of one of the author's official duties as an Employee of the United States Government and is therefore a work of the United States Government. In accordance with 17 U.S.C. 105, no copyright protection is available for such works under U.S. Law.

Public Domain Mark 1.0

<https://creativecommons.org/publicdomain/mark/1.0/>

Access to this work was provided by the University of Maryland, Baltimore County (UMBC) ScholarWorks@UMBC digital repository on the Maryland Shared Open Access (MD-SOAR) platform.

Please provide feedback

Please support the ScholarWorks@UMBC repository by emailing scholarworks-group@umbc.edu and telling us what having access to this work means to you and why it's important to you. Thank you.

Achieving high flux amplification in a gun-driven, flux-core spheromak

To cite this article: E.B. Hooper *et al* 2007 *Nucl. Fusion* **47** 1064

View the [article online](#) for updates and enhancements.

You may also like

- [Effect of geometric and magnetic boundary conditions on magnetic islands in 3D force-free ideal MHD equilibria](#)
T.E. Benedett and C.J. Hansen
- [Sustained Spheromak Physics Experiment \(SSPX\): design and physics results](#)
E B Hooper, R H Bulmer, B I Cohen et al.
- [Relativistic Magnetic Explosions](#)
Maxim V. Barkov, Praveen Sharma, Konstantinos N. Gourgouliatos et al.

Achieving high flux amplification in a gun-driven, flux-core spheromak

E.B. Hooper, D.N. Hill, H.S. McLean, C.A. Romero-Talamás and R.D. Wood

Lawrence Livermore National Laboratory, Livermore, CA 94551, USA

Received 27 February 2007, accepted for publication 11 June 2007

Published 3 August 2007

Online at stacks.iop.org/NF/47/1064

Abstract

A new means of operating flux-core spheromaks with possibly increased stability, confinement and pulse length is analysed by a resistive magnetohydrodynamic (MHD) model. High amplification of the bias poloidal flux, required to minimize ohmic losses, is achieved by reducing the bias rapidly in a plasma formed at a lower amplification. The plasma separatrix is predicted to expand and incorporate the removed bias flux maintaining the total poloidal flux within the spheromak's flux-conserving wall. MHD energy on open magnetic field lines is reduced, reducing magnetic fluctuation levels. A means of experimental verification is suggested that may point the way to fusion-relevant spheromaks.

PACS numbers: 52.55.Ip, 52.30.Cv

(Some figures in this article are in colour only in the electronic version)

1. Introduction

The flux-core spheromak has a toroidal magnetic confinement geometry formed in an axisymmetric, simply-connected magnetic flux conserver. An applied (bias) poloidal flux and electric current from an electrode ('gun') thread the hole in the torus and are amplified by a dynamo effect, in principle to an arbitrary level [1], generating a steady component of the toroidal current in a nearly axisymmetric magnetic geometry without the flux limits of a transformer. As discussed later, however, experiments and modelling find that amplification by the dynamo saturates at a low enough level that resistive losses in the open field line, edge plasma dominate the power balance of the spheromak. These losses must be reduced to a relatively low level for spheromaks to make attractive, high-temperature experiments or reactors. In addition to observations on the sustained spheromak physics experiment (SSPX) [2] which are discussed in more detail in this paper, saturation has also been seen in the compact toroid experiment (CTX) [3], the flux amplification toroid (FACT) [4] and the spheromak experiment (SPHEX) [5, 6].

Resistive magnetohydrodynamic (MHD) modelling is used here to analyse a new method (*active bias-reduction*, ABR) of achieving high amplification following an initial low-amplification phase, thereby reducing the resistive losses on open field lines and potentially offering a significant step towards fusion-quality spheromak plasmas. ABR extends helicity injection from a coaxial gun (CHI) [7], e.g. as used in SSPX [2, 8] to form spheromak plasmas. The MHD code

used in this study, NIMROD [9], has been benchmarked against SSPX [10, 11] which is researching a range of physics including flux and current amplification [2], the role of magnetic fluctuations in the formation and confinement of the spheromak plasma [12], and magnetic reconnection generating the conversion of injected toroidal flux into poloidal flux [13]. For a review of previous spheromak research see Jarboe [7] and references therein.

The spheromak has a number of features which make it a potentially attractive fusion-energy device. An axisymmetric, simply connected flux conserver surrounds the plasma with no toroidal-field coils along the magnetic axis, yielding a compact system so a spheromak should be easier to maintain than the tokamak and stellarator. The use of helicity injection to drive and sustain a toroidal current without a transformer provides additional simplicity, including a natural divertor. The trade-off is an increase in physics complexity. Furthermore, increasing and sustaining current parallel to the magnetic field by helicity transport into the spheromak requires that magnetic surfaces be open at least part of the time [14], with significant consequences for energy confinement which may require separation of the current drive and confinement phases in a reactor [15]. The spheromak current and flux will decay during the confinement phase as the dynamo is turned off, so it will likely be necessary to rebuild them periodically using a dynamo pulse. Experiments in SSPX exploring the physics of helicity injection into a slowly decaying spheromak [16] to rebuild the plasma thus complement the present flux-amplification concept by developing a technique to extend the plasma duration.

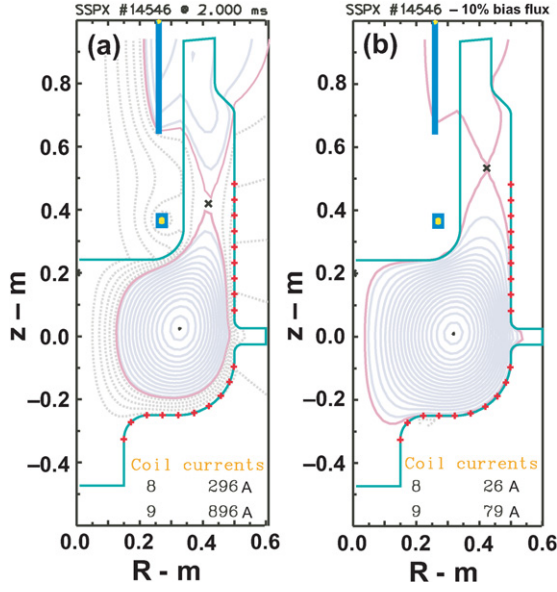


Figure 1. (a) Spheromak (SSPX) axisymmetric equilibrium with $\lambda_g = 9.3 \text{ m}^{-1}$ and flux amplification 3.3. (b) Axisymmetric equilibrium with reduced bias flux at fixed λ_g yielding flux amplification = 32.4. The flux conserver surrounds the plasma, and the bias flux is generated by the external coils.

In this paper, we first consider experimental, flux amplification results in SSPX. These provide the motivation for the modelling which follows. A two-dimensional (2D) model is used to explore flux amplification by ABR; this allows the basic concept to be examined without the complexity associated with the full three-dimensional (3D) problem. Furthermore, the 2D analysis can be done rapidly and can be used to explore the consequences of changing parameters or geometry. A 3D time history using a resistive MHD simulation follows and includes the effects of symmetry-breaking modes and instabilities. Although the number of 3D simulations is limited by the long computational times needed, this confirms the results of the 2D analysis. Interestingly, the mode energies are predicted to be significantly reduced from those in the initial, low flux-amplification spheromak. The concluding section includes a first step (using the 2D approximation) towards the design of an experimental geometry for implementing this concept. Details of such a design are left to future work.

2. Flux amplification in SSPX

A flux-core spheromak for a high-temperature confinement experiment or reactor will require a bias poloidal flux amplification of 50–100, primarily to minimize the volume of open field lines to keep ohmic losses in the edge from dominating the power balance [17]. Consider the two SSPX MHD equilibria in figure 1. These were generated by solving the Grad–Shafranov equation using the Corsica code [8] in the SSPX geometry, used in this study as spheromaks in it are well characterized. The equilibrium in figure 1(a) is a fit to an experimental discharge with $\lambda = \mu_0 \mathbf{j} \cdot \mathbf{B} / B^2$ assumed spatially constant but chosen to optimize the fit to experimental measurements; \mathbf{j} is the current density, and \mathbf{B} is the magnetic

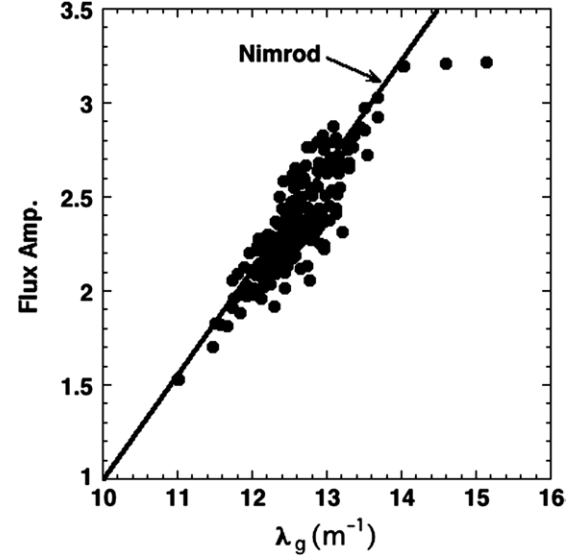


Figure 2. Flux amplification in the SSPX experiment and simulations. The experimental results (●) are the ratio of the achieved flux on the magnetic axis to the applied bias flux. A Bessel-function model is used to calculate the achieved flux from magnetic field measurements in the experiment. The plotted points used formation pulses long enough for the amplification to approach saturation; bias flux range = 40–74 mWb, gun current range = 0.50–0.72 MA. The line fitting simulation results (labelled ‘NIMROD’) use a long, constant-current pulse and 50 mWb bias flux, and reach saturation.

field. (The constant- λ approximation is relaxed in the 3D simulations.) The equilibrium in figure 1(b) was found by reducing the bias flux at fixed $\lambda_g = \mu_0 I_g / \Psi_g$, with I_g the gun current and Ψ_g the effective applied bias flux (which is also the flux on the separatrix), and fixed Ψ_0 , the poloidal flux between the magnetic and geometric axes. The cross section area of the edge plasma, between the separatrix and geometric axis or wall, scales inversely as the flux amplification, Ψ_0 / Ψ_g .

High amplification is essential for efficient operation of future spheromak experiments. The edge fieldline connections to material surfaces result in a low ($\sim 30 \text{ eV}$) edge electron temperature with correspondingly large ohmic losses. (Helicity-injection techniques that drive current on fieldlines outside the separatrix [18] which do not reach material surfaces may yield higher temperatures.) Increasing the flux amplification at fixed λ_g thus reduces the ohmic power loss proportionally. (The simulations will show that the area of open fieldlines is proportional to the bias flux so for these results the current density is unchanged if λ_g is constant. The electron temperature on open fieldlines [19] is insensitive to the bias flux, so power losses approximately scale as the flux amplification.)

Experimental results to date typically achieve flux amplifications of about 3–4, although up to 6 has been obtained. Experimental results are compared with resistive MHD simulations [15] in figure 2; the reason for the apparent flattening of the amplification above 14 m^{-1} in these discharges is unclear. The current amplification is defined as the ratio of toroidal current in the flux conserver to the gun current and is approximately 1/2 the flux amplification. The observed threshold dependence on λ_g is consistent with the Kruskal–Shafranov condition for instability of a plasma column, which

is $\lambda_g > 4\pi/L$ with L the effective length of the column. The numerical factor will be different in SSPX; it is reduced if one or both ends of the column are not line-tied [20], and the effective length of the column in SSPX is longer than the flux-conserver height due to the coaxial gun, so the agreement of this simple condition with experiment is semi-quantitative, as in other spheromaks [5, 21].

Experiments on SPHEX explored flux amplification in some detail and yielded an empirical equation for the poloidal field strength, B_p , at an equatorial wall probe [6]. Although this equation has a somewhat different form than the offset linear result shown for SSPX, the ratios of B_p to bias flux are similar. As examples: A SPHEX high-current data point in figure 4 of [6] has $\lambda_g = 27 \text{ m}^{-1}$, $B_p = 0.09 \text{ T}$ and $\Psi_g = 0.048 \text{ Wb}$, so $B_p/\Psi_g = 21 \text{ T Wb}^{-1}$. The SSPX data point at $\lambda_g = 14.0 \text{ m}^{-1}$ in figure 2 had $B_p = 0.46 \text{ T}$ and $\Psi_g = 0.048 \text{ Wb}$ so $B_p/\Psi_g = 9.6 \text{ T Wb}^{-1}$; at $\lambda_g = 27 \text{ m}^{-1}$ the simulations [15] predict $B_p/\Psi_g = 31 \text{ T Wb}^{-1}$. The different scaling deduced for the two experiments may result from the operational differences: SPHEX was operated in a ‘bubble-burst’ mode with the flux ejected from the gun only when the gun current exceeded a threshold, whereas in SSPX much of the bias flux exits the gun at zero gun current. In any event, both experiments saturated at low flux amplifications.

The detailed reasons for the flux amplification saturation at fixed λ_g are not well understood. Modelling of the column mode in SPHEX [22] suggests that the coupling to the spheromak limits its amplitude and can even stabilize the mode intermittently, but full stabilization has not been observed in SSPX or its simulations. Saturation of flux amplification has also been found in a hyper-resistive model of the spheromak in which the column mode is not explicitly included [23], exhibiting a balance between helicity injection and resistive losses [24]. In any event, it is clear that the gun voltage and thus the helicity injection rate, $\dot{K}_{\text{inj}} = 2\Psi_g V_g$, are determined by λ_g . In experiments it is seen that the magnitude of the gun voltage increases with λ_g [15, 24]. The voltage spikes generated by the reconnection events, seen clearly in simulations [13] which do not have confounding effects (e.g. at the cathode surface), have higher amplitude and a faster repetition rate at the higher λ_g in both simulation and experiment. Figure 3 shows the gun voltages and the energy in the $n = 1$ mode for two of the simulations used in figure 2. the greater rate of helicity injection at higher λ_g results in greater (but saturated) magnetic energy in the flux conserver as noted in the caption to figure 3.

In principle, we might obtain high flux amplification by going to high λ_g . Our simulations have found no limit to flux amplification with λ_g , and saturation in SSPX experiments (e.g. two points in figure 2) may result from wall interactions or other ‘kitchen’ physics so further experiments are needed to explore this issue. Extrapolating figure 2 to an amplification of 50 yields $\lambda_g = 96 \text{ m}^{-1}$; at bias fluxes of 30–75 mWb, typical of good operation in SSPX, this requires $I_g = 2.3$ – 5.7 MA . These very high gun currents (and powers) would damage the gun and generate significant impurities, and are not very practical. Furthermore, solutions of the Grad–Shafranov equation for SSPX [8], fitted to experimental magnetic probe measurements, show that a large value of λ on the edge of the mean-field (azimuthally averaged) spheromak results in a large λ -gradient with a deep minimum on the (mean-field) magnetic

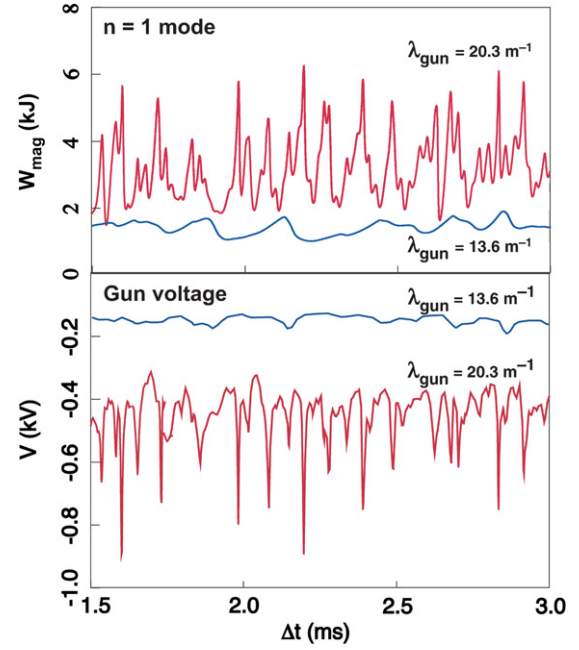


Figure 3. Total magnetic energy from NIMROD simulations within the flux conserver for the $n = 1$ column mode (upper figure) and gun (cathode) voltage (lower figure) during sustainment at $\lambda_g = 20.3 \text{ m}^{-1}$ (‘spiky’ traces) and 13.6 m^{-1} (‘smooth’ traces). The energies in the $n = 0$ (axisymmetric) modes are 370 kJ and 82 kJ, respectively.

axis. The corresponding safety factor, q , crosses unity near the magnetic axis if the spheromak is driven strongly enough, and would likely drive strong $n=1$ interior oscillations if the nearly symmetric equilibrium were a good approximation to this state. (Note that q always crosses unity near the separatrix if it is <1 inside it.) In fact, detailed probe measurements in SPHEX [5, 25] show a highly nonaxisymmetric, nonlinear structure develops in strongly driven spheromaks. Although experiments have never reached high amplification, this large departure from symmetry suggests that the resulting spheromak would be of poor quality.

As an alternative to the present approach, one could ramp the gun current to zero, eliminating edge ohmic losses. In practice, however, this causes q to pass through $1/2$ in the flux-core spheromak, resulting in a virulent $n = 2$ mode. This mode terminates most discharges in SSPX when the power supply current drops at the end of the pulse and was first studied in CTX [26]. The advantage of ABR is that it maintains the edge boundary condition, thus preventing q from crossing $1/2$ (except possibly close to the separatrix). Also, although not explored here, it may be possible to optimize operation by adjusting the value of λ_g during ABR.

3. Flux amplification using active bias reduction: 2D model

Experiments and simulations thus suggest that it will be very difficult to obtain high flux amplification simply by driving the gun for a long time at high current. Instead, we consider an alternative approach, ABR. A high current spheromak is formed, e.g. as in conventional CHI. The bias flux and

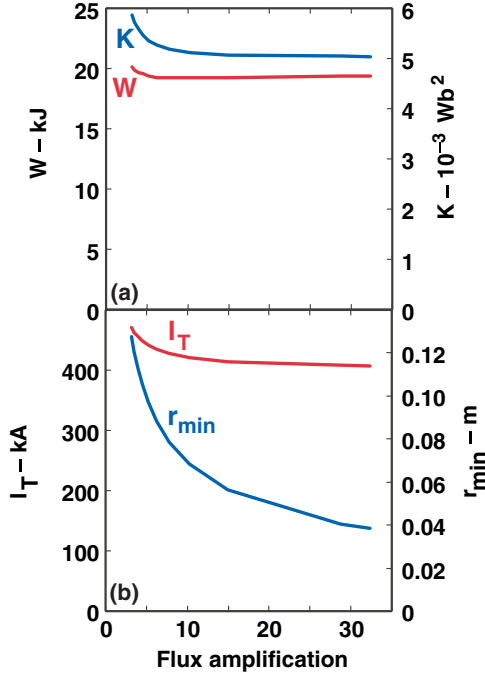


Figure 4. Flux amplification scaling in the axisymmetric model of (a) magnetic energy, W , and helicity, K , and (b) toroidal current, I_T , and minimum separatrix radius, r_{\min} .

gun current are then reduced together to low values while maintaining their ratio constant, thus maintaining the edge boundary condition in λ needed for global stability. The 3D simulations below show that the total poloidal flux and toroidal current in the flux-conserver remain approximately constant during this process so the flux amplification increases while the ohmic edge losses decrease. The poloidal flux and current within the spheromak separatrix increase as it expands to include more of the flux-conserver volume. An additional advantage will be seen to be a significant reduction of the amplitude of MHD modes driven by the gun current. As a result, the spheromak plasma is better confined and hotter in the subsequent, high-temperature phase [12] than in the absence of ABR.

Before describing the resistive, 3D MHD simulation of ABR, consider an axisymmetric approximation. The highly conducting flux conserver in the present experiment will not allow the bias magnetic flux to be reduced on the discharge time scale, but we assume that modifications, such as a vertical cut in the gun wall, allow the axisymmetric bias flux to be changed rapidly. The gun current and bias flux are changed together, so that λ_g is constant during the process. In experiments and simulations the total poloidal flux, Ψ_0 , is generated from injected toroidal flux by reconnection events associated with the dynamo [13], but we assume that there is no dynamo during the bias flux change so the poloidal flux on the magnetic axis of the spheromak is constant. (Resistive MHD simulations, discussed in the following section, guided this assumption.)

An initial equilibrium is shown in figure 1 along with the result of increasing the flux amplification by a factor of 10 at constant λ_g . The scaling of spheromak parameters during this change is shown in figure 4. Note that the magnetic energy and helicity decrease somewhat as the gun flux and

current are reduced at constant total poloidal flux. During a discharge the injected power and rate-of-helicity are $\dot{W}_{\text{inj}} = I_g V_g$ and $\dot{K}_{\text{inj}} = 2\Psi_g V_g$, so the part of the gun voltage, V_g , generating stored energy and helicity will reverse sign. (The total voltage includes ohmic losses on open field lines and, in the experiment, a drop across the sheath [24].) The toroidal current also drops slightly. We can estimate the vertical magnetic field on the geometric axis as $\sim \mu_0 I_T f / 2\pi R_0$ where $f = 1$ assumes that the toroidal current is concentrated at the magnetic axis, and $f \sim 1$ results from a distributed current, so $I_T \approx \text{constant}$ implies that the vertical field near the geometric axis is approximately constant during the process. The minimum radius of the separatrix then scales as $\Psi_g^{1/2}$, close to that seen in the calculation. The edge ohmic losses decrease approximately proportional to the gun current and thus proportional to Ψ_g , a factor of 10 in this example.

4. Flux amplification using active bias reduction: 3D simulation

Resistive MHD modelling is used for a 3D simulation of ABR with the spheromak poloidal flux calculated self consistently. The simulation used similar parameters to those in [11, 13] including high parallel thermal conductivity and a perpendicular thermal conductivity coefficient similar to measurements in SSPX [12], toroidal modes 0–5, and kinetic viscosity of $1000 \text{ m}^2 \text{ s}^{-1}$. Comparisons of simulations with experiment find that these give a reasonably good approximation to observations for many of the important physics parameters, as discussed in the previous publications. Unpublished simulations find that the energies in modes with $n > 5$ generally drop off as $n^{-\alpha}$, with the value of α depending on the viscosity model and other parameters, but generally > 4 . Furthermore, the mode amplitudes are small, typically a few per cent or less than the energy in the axisymmetric magnetic field. Thus, although including higher order modes in the simulation will result in quantitative changes, these are small with minimal qualitative effects.

A discharge is established at constant bias flux, resulting in the azimuthally averaged equilibrium shown in figure 5(a). The bias and gun current are then reduced over 1 ms with the time dependence shown in figure 6(a), resulting in the equilibrium in figure 5(b). Figure 6(b) shows the gun voltage and figure 6(c) the toroidal current and total energy in the flux conserver throughout this time. The total energy, which is primarily in the magnetic field, drops during ABR consistent with the reduction in power input.

The azimuthally averaged poloidal flux surfaces at the start and end of the ramp down can be compared with those in figure 1; the minimum radius of the separatrix goes from 0.075 m to 0.02 m, again in agreement with the approximate $\Psi_g^{1/2}$ scaling. The detailed magnetic structures in the coaxial gun differ, but otherwise the behaviour is nearly the same. The poloidal flux on the magnetic axis drops a bit, by an amount consistent with resistive decay of the toroidal current. As was assumed in the 2D model, the spheromak separatrix expands to include most of the initial edge flux.

The NIMROD simulation includes the resistive voltage drop although not a sheath voltage, and the net voltage is positive throughout most of the pulse although its sign reverses

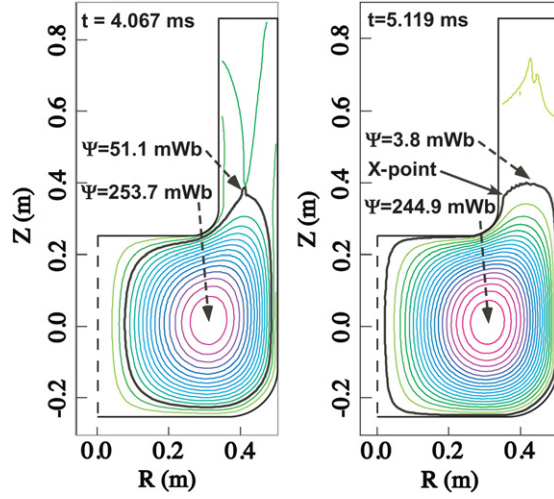


Figure 5. Poloidal flux (toroidally averaged) surfaces from a 3D resistive MHD simulation of bias flux reduction with a flux amplification change from 5.0 to 64.4; $\lambda_g = 13.6 \text{ m}^{-1}$. (a) Initial equilibrium. (b) Equilibrium at the end of the flux reduction.

when the gun current and flux are changing the most rapidly. At the beginning of the pulse, the resistive voltage drop is $V_g = I_g \eta \ell / A$, where η is the resistivity and ℓ and A are appropriate averages of the current path length and edge area. At 25 eV, $\ell \approx 1 \text{ m}$, and $A \approx 0.03 \text{ m}^2$, $V_g \approx 100 \text{ V}$, in rough agreement with figure 5(b). The voltage ‘jumps’ at about 4.9 ms result when the position at which the separatrix connects to the gun wall switches from high in the gun (figure 5(a)) to low in the gun (figure 5(b)). The separatrix X-point moves to the gun wall near an X-point in the bias magnetic field; the separatrix in figure 5(b) shows a break at this location, near the gun wall just below 0.4 m.

Following ABR the simulation is continued to $t \approx 10 \text{ ms}$ with the gun current reduced in the simulation by a constant factor of 12.9. The gun voltage is approximately constant at 60 V during this time and there is no indication of reconnection events or helicity drive of the spheromak. The azimuthally averaged and $n = 1$ magnetic energies are compared in figure 7 with those in the absence of ABR; the averaged energy differs little but the $n = 1$ energy is significantly reduced. This is consistent with a qualitative picture in which the column mode is coupled to the spheromak which is stabilized to the tilt and shift ($n = 1, m = 1$) modes by the flux conserver geometry. Although the Kruskal–Shafranov condition for an isolated column has not been affected as λ_g is constant, the free energy available to drive the mode is reduced at lower gun current, thereby likely yielding the lower amplitude. Indeed, this low amplitude suggests that the mode is stable and driven only by mode coupling during this time. After about 1 ms the amplitude of the $n = 1$ column mode increases, but its amplitude is still significantly reduced from the original value, by ~ 35 in this example.

The energies in modes 2–5 are compared in figure 8 for the ABR and non-ABR simulations. They are generally reduced in the latter case. The primary consequence of the symmetry breaking modes is to generate stochastic regions of the magnetic field and thus reduce the volume of ‘good’ magnetic surfaces required for energy confinement; see [9, 10]

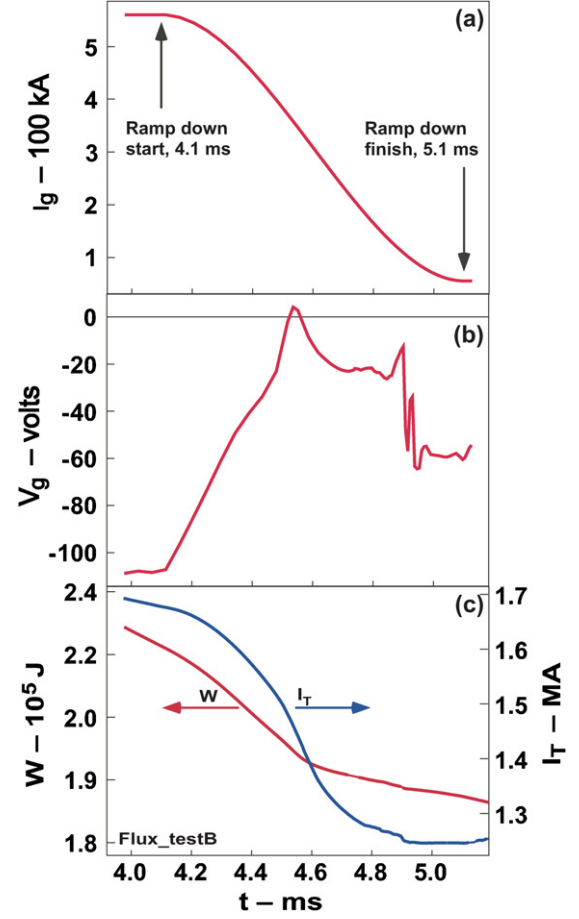


Figure 6. (a) Ramp-down of gun current, I_g , (b) gun (cathode) voltage, V_g , (c) magnetic energy, W , and toroidal current, I_T ; note the suppressed zeros in (c). In this simulation, the ramp-down of the bias flux had the same time dependence as the gun current.

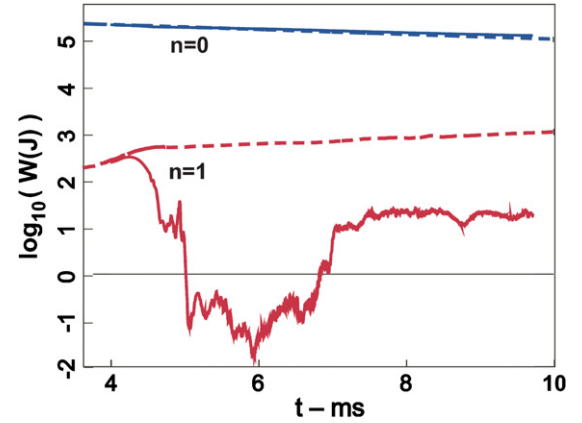


Figure 7. Magnetic energy in the $n = 0$ (axisymmetric) and $n = 1$ modes with (—) and without ABR (---). λ_g is constant (13.6 m^{-1}) during both evolutions.

for examples. The volume of good surfaces is increased in the simulated ABR plasma relative to the lower amplitude spheromak, thus improving energy confinement. After about 8 ms in the non-ABR simulation there are strong $2/3$ magnetic islands near the magnetic axis and a significant volume of stochastic magnetic fieldlines which allow large thermal losses.

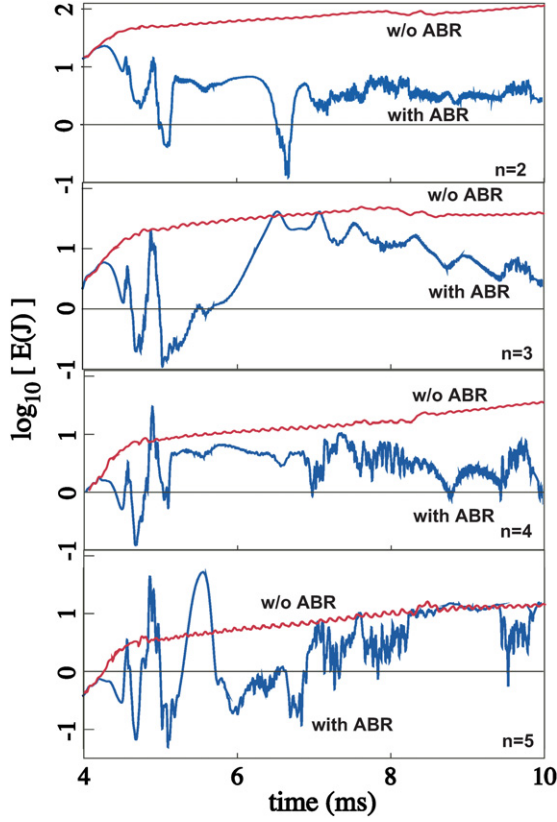


Figure 8. Mode energies in simulations with and without ABR.

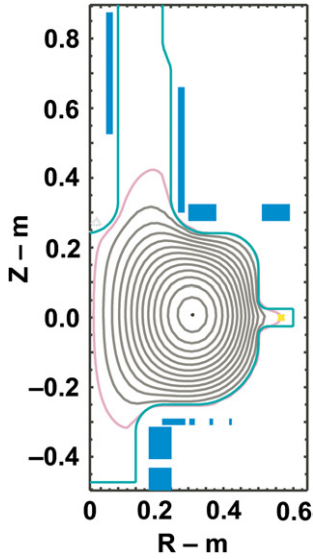


Figure 9. Preliminary design for a new flux conserver and gun. Flux amplification = 41.

The reduced activity in the ABR case results in a calculated peak- electron temperature in the simulation of $T_e \approx 170$ eV, two to three times that in the non-ABR example.

5. Experimental considerations and summary

Experiments studying ABR will require a flux conserver that differs from those presently in use to allow for rapid changes in

magnetic flux demanded by this new scenario. An example of a possible design is shown in figure 9. Bias poloidal flux enters the flux conserver through the gap in the gun at the top and exits through the hole in the bottom. The external coils are adjusted such that the shape of the outer vacuum flux surface closely follows the contour of the flux conserver. For the flux to be changed on a fast (millisecond) time, the walls of the gun will have to have a vertical slot or the magnets will need to be inside the gun walls. As the magnetic energy within the flux conserver decreases only slightly during ABR, the magnetic energy to be removed is that in the gun and exit volumes; for each, $W_0 \approx \Psi_g^2 / 2\mu_0 \pi a^2 L$ with a and L the characteristic radius and length of a section. The voltage required is $V \approx 2W_0 / I_0 \tau$, with τ the characteristic ABR time. At $\Psi_g = 50$ mWb, $a = 0.2$ m, and $L = 0.5$ m, $W_0 = 16$ kJ; if $I_0 = 1$ kA and $\tau = 1$ ms, $V \approx 15$ kV. Detailed design would undoubtedly change these, but the numbers given here suggest that the eventual parameters will be reasonable for an experiment although careful bias-coil design will be needed. A larger flux conserver may have higher T_e , allowing a longer ABR evolution time, although detailed modelling will be required to explore this scaling.

ABR is also consistent with the control of the tilt and shift modes by feedback stabilization such as an ‘intelligent’ wall [27] rather than by a highly conducting flux conserver. Recent experimental studies in the reversed-field pinch with a thin, resistive wall demonstrate successful active stabilization of non-resonant resistive wall modes and locking of resonant tearing modes over the duration of the discharge [28]. Detailed examination of this physics in the spheromak is beyond the present study.

In conclusion, both experiments and simulations suggest that it will be very difficult to achieve high flux and current amplification in a conventional, helicity-injected spheromak. The injection would have to be driven extremely ‘hard’ (with the gun current \gg the threshold in λ_g) likely damaging electrodes and perhaps generating such a high degree of asymmetry that a good spheromak cannot be formed. We are thus motivated to find a new approach to achieving flux amplification. The present concept, Active Bias Reduction, is considered in that context.

Resistive MHD modelling of flux amplification in a flux-core spheromak predicts that ABR has additional benefits. The plasma stability is improved with reduced ohmic losses on open field lines. The amplitudes of resonant magnetic modes are reduced, resulting in improved magnetic surfaces and reduced thermal losses. Such an approach would also be consistent with an advanced spheromak experiment, e.g. using feedback stabilization rather than a highly conducting flux conserver.

Further experiments and simulations will also be required to address issues such as the likely requirement to achieve long pulses by regularly rebuilding the decaying spheromak current, as mentioned in the Introduction.

The modelling indicates that an axisymmetric, quasi-static model using the Grad–Shafranov equation can be used to explore the MHD evolution of these plasmas, allowing fast exploration of experimental options. Resistive MHD modelling will be important for optimization, e.g. by exploring the sensitivity of stability to the value of λ_g following ABR. The results obtained in this report suggest that ABR is a mechanism for achieving high flux amplification, one of the requirements

for significant progress towards a fusion-quality plasma in a spheromak.

Acknowledgments

The approach to flux amplification analysed here arose from discussions with T.K. Fowler. C.R. Sovinec's guidance was essential in modifying NIMROD for the ABR calculations. Careful reading and comments by B.I. Cohen and E.J. Synakowski are gratefully acknowledged. Discussions with many colleagues, including L.L. LoDestro, L.D. Pearlstein and D.D. Ryutov, have helped form our understanding of spheromaks. This work was performed under the auspices of the US Department of Energy under contract W7405-ENG-48 at the University of California Lawrence Livermore National Laboratory.

References

- [1] Taylor J.B. and Turner M.F. 1989 *Nucl. Fusion* **29** 219
- [2] Wood R.D., Hill D.N., Hooper E.B., Woodruff S., McLean H.S. and Stallard B.W. 2005 *Nucl. Fusion* **45** 1582
- [3] Jarboe T.R., Henins I., Sherwood A.R., Barnes C.W. and Hoida H.W. 1983 *Phys. Rev. Lett.* **51** 39
- [4] Nagata M., Kanki T., Matsuda T., Naito S., Tatsumi H. and Uyama T. 1993 *Phys. Rev. Lett.* **71** 4342
- [5] Duck R.C., Browning P.K., Cunningham G., Gee S.J., al-Karkhy A., Martin R. and Rusbridge M.G. 1997 *Plasma Phys. Control. Fusion* **39** 715
- [6] Rusbridge M.G., Gee S.J., Browning P.K., Cunningham G., Duck R.C., al-Karkhy A., Martin R. and Bradley J.W. 1997 *Plasma Phys. Control. Fusion* **39** 683
- [7] Jarboe T.R. 1994 *Plasma Phys. Control. Fusion* **36** 945
- [8] Hooper E.B., Pearlstein L.D. and Bulmer R.H. 1999 *Nucl. Fusion* **39** 863
- [9] Sovinec C.R., Gianakon T.A., Held E.D., Kruger S.E., Schnack D.D. and NIMROD Team 2003 *Phys. Plasmas* **10** 1727
- [10] Sovinec C.R., Cohen B.I., Cone G.A., Hooper E.B. and McLean H.S. 2005 *Phys. Rev. Lett.* **94** 035003
- [11] Cohen B.I., Hooper E.B., Cohen R.H., Hill D.N., McLean H.S., Wood R.D., Woodruff S., Sovinec C.R. and Cone G.A. 2005 *Phys. Plasmas* **12** 056106
- [12] McLean H.S., Wood R.D., Cohen B.I., Hooper E.B., Hill D.N., Moller J.M., Romero-Talamás C. and Woodruff S. 2006 *Phys. Plasmas* **13** 056105
- [13] Hooper E.B., Kopriva T.A., Cohen B.I., Hill D.N., McLean H.S., Wood R.D., Woodruff S. and Sovinec C.R. 2005 *Phys. Plasmas* **12** 092503
- [14] Boozer A.H. 1993 *Phys. Fluids B* **5** 2271
- [15] Hooper E.B., Cohen B.I., Hill D.N., LoDestro L.L., McLean H.S., Romero-Talamás C.A. and Wood R.D. 2007 *J. Fusion Energy* **26** 71
- [16] Woodruff S., Stallard B.W., McLean H.S., Hooper E.B., Bulmer R., Cohen B.I., Hill D.N., Holcomb C.T., Moller J. and Wood R.D. 2004 *Phys. Rev. Lett.* **93** 205002
- [17] Hagenston R.L. and Krakowski R.A. 1985 *Fusion Technol.* **8** 1606
- [18] Sieck P.E., Jarboe T.R., Izzo V.A., Hamp W.T., Nelson B.A., O'Neill R.G., Redd A.J. and Smith R.J. 2006 *Nucl. Fusion* **46** 254
- [19] Hooper E.B., Cohen R.H. and Ryutov D.D. 2000 *J. Nucl. Mater.* **278** 104
- [20] Ryutov D.D., Furno I., Intrator T.P., Abbate S. and Madziwa-Nussinov T. 2006 *Phys. Plasmas* **13** 032105
- [21] Turner W.C., Goldenbaum G.C., Granneman E.H.A., Hammer J.H., Hartman C.W., Prono D.S. and Taska J. 1983 *Phys. Fluids* **26** 1965
- [22] Brennan D., Browning P.K., Van der Linden R.A.M., Hood A.W. and Woodruff S. 1999 *Phys. Plasmas* **6** 4248
- [23] Hooper E.B. and Pearlstein L.D. 2002 *Plasma Phys. Rep.* **28** 765
- [24] Stallard B.W., Hooper E.B., Woodruff S., Bulmer R.H., Hill D.N., McLean H.S., Wood R.D. and SSPX Team 2003 *Phys. Plasmas* **10** 2912
- [25] Woodruff S. and Negata M. 2002 *Plasma Phys. Control. Fusion* **44** 2539
- [26] Knox S.O., Barnes C.W., Marklin G.J., Jarboe T.R., Henins I., Hoida H.W. and Wright B.L. 1986 *Phys. Rev. Lett.* **56** 842
- [27] Bishop C.M. 1989 *Plasma Phys. Control. Fusion* **31** 1179
- [28] Brunzell P.R., Kuldkepp M., Menmuir S., Ceconello M., Hedqvist A., Yadikin D., Drake J.R. and Rachlew E. 2006 *Nucl. Fusion* **46** 904